

Hybrid Monte Carlo/deterministic activation calculation to support the decommissioning of PWRs:  
Validation against data from the thermal shield of the Enrico Fermi NPP

*Original*

Hybrid Monte Carlo/deterministic activation calculation to support the decommissioning of PWRs: Validation against data from the thermal shield of the Enrico Fermi NPP / Bleyrat, S., Dulla, S., Pancotti, F., Ricci, L., Vicini, C., Zanino, R.. - In: ANNALS OF NUCLEAR ENERGY (ONLINE). - ISSN 1873-2100. - ELETTRONICO. - 181:(2023), pp. 1-12.  
[10.1016/j.anucene.2022.109527]

*Availability:*

This version is available at: 11583/2972932 since: 2022-11-09T14:34:15Z

*Publisher:*

Elsevier

*Published*

DOI:10.1016/j.anucene.2022.109527

*Terms of use:*

This article is made available under terms and conditions as specified in the corresponding bibliographic description in the repository

*Publisher copyright*

Elsevier postprint/Author's Accepted Manuscript

© 2023. This manuscript version is made available under the CC-BY-NC-ND 4.0 license  
<http://creativecommons.org/licenses/by-nc-nd/4.0/>. The final authenticated version is available online at:  
<http://dx.doi.org/10.1016/j.anucene.2022.109527>

(Article begins on next page)

# **Hybrid Monte Carlo/deterministic activation calculation to support the decommissioning of PWRs: validation against data from the thermal shield of the Enrico Fermi NPP**

S. Bleynat <sup>a</sup>, S. Dulla <sup>a</sup>, F. Pancotti <sup>b</sup>, L. Ricci <sup>b</sup>, C. Vicini <sup>b</sup>, R. Zanino <sup>a</sup>

<sup>a</sup> NEMO group, Dipartimento Energia, Politecnico di Torino, Corso Duca degli Abruzzi 24, 10129 Torino - Italy

<sup>b</sup> Sogin, Via Marsala, 51/c, 00185 Roma - Italy

Corresponding author: [simone.bleynat@polito.it](mailto:simone.bleynat@polito.it)

## Abstract

## 1 Introduction

## 2 Development of the calculation scheme

### 2.1 Critical Simulation: source generation (STEP 1)

### 2.2 External source simulations: accelerated transport and variance reduction techniques (STEP 2)

### 2.3 Activation calculation (STEP 3)

#### 2.3.1 Highly detailed material compositions, including the impurities

#### 2.3.2 Reconstructed irradiation history and decay time

#### 2.3.3 Nuclear data

#### 2.3.4 Neutron spectra and integral neutron flux

### 2.4 Results comparison and validation (STEP 4)

#### 2.4.1 1969 sampling campaign

##### 2.4.1.1 Axial distribution of the residual activation caused by $^{54}\text{Mn}$ and $^{60}\text{Co}$ at $\theta = 0^\circ$

##### 2.4.1.2 Other local values of the residual activation on the thermal shield surfaces

#### 2.4.2 1992 sampling campaign

## 3 Conclusions and perspectives

## 4 Acknowledgements

## 5 References

## **Abstract**

The progressive aging of nuclear power plants (NPPs) in the world is a relevant issue for the nuclear industry. The radiological characterization of the reactor is usually performed using a combination of sampling campaigns and computer simulations, and the latter are particularly useful if measurements are limited.

This paper describes the development of a four-step, hybrid Monte Carlo/deterministic calculation scheme to evaluate the residual activation of a pressurized water reactor, focusing the analysis on the Enrico Fermi power plant in Italy. The scheme performance is evaluated using the ratio between the calculated specific activities and the measured ones (C/M ratio) for each point and isotope considered. The overall performance is satisfactory, as the scheme provides conservative results with a good accuracy, without excessive overestimations. The present computational scheme can be adapted to study the lifetime of a NPP, thus providing a useful support tool for the dismantling process in NPPs.

## **Keywords:**

Decommissioning, Activation, Monte Carlo, Serpent, FISPACT

## **1. Introduction**

The ageing process of the world-wide nuclear power reactor fleet is an issue that will increasingly need to be addressed in the coming decades, as there are currently more than 400 nuclear power reactors in operation in the world, and a large fraction of these plants (around 65%) was built before the end of the 1980s (IAEA, 2022). Worldwide, 200 nuclear reactors have been permanently shut down, and are either decommissioned or at various stages of the decommissioning (IAEA, 2022).

Italy invested early in the development of a civil nuclear power industry, and the first nuclear power plant (NPP), built near Latina, began operating in 1963. The chosen design was a gas cooled-graphite moderated reactor (MAGNOX). Shortly afterwards, a boiling water reactor (BWR) started operating in Sessa Aurunca (1964), and a pressurized water reactor (PWR) at the Enrico Fermi NPP in Trino began operation in 1965. The design used for the latter plant was an upscale of the PWR built for the US Yankee Rowe power plant. An additional plant based on the BWR technology was built in Caorso in the following years and started operating in 1981 as a response to the rapidly growing energy demand. The Chernobyl accident (1986) and the ensuing referendum vote (1987) have effectively halted the production of nuclear energy in Italy, leading to the immediate final shutdown of the Latina NPP, the stop of the construction of the new Montalto di Castro NPP in 1989 and the final shutdown of the Trino and Caorso NPPs in 1990. The Garigliano NPP had already been permanently shut down since 1978. All the four above-mentioned Italian nuclear plants and other nuclear-related facilities are currently in various stages of decommissioning.

The deployment of a comprehensive decommissioning plan is a complex, multidisciplinary engineering process, and the optimization of decommissioning strategies requires a thorough knowledge of the plant, of its operational history and its radiological status. In particular, the

availability of a radiological inventory of structures and components, in terms of activation and contamination data, is useful to optimize the design of the dismantling phases, the workers exposure, the waste classification and management and consequently the decommissioning cost. Building this radiological inventory can be quite challenging and often requires, after shutdown, laborious characterization campaigns. The activation of the structures and components surrounding the core such as the Reactor Vessel Internals (RVIs) and the Reactor Pressure Vessel (RPV), however, can be obtained by numerical simulation, validating the outcomes with available measurements of detectors/samples obtained during the operation (i.e. vessel fluence monitoring program). This approach overcomes the necessity of new sampling plans, avoiding unnecessary workers exposure and additional costs, and allows to perform confirmation measurements directly during the on-going dismantling activities.

Usually, the numerical simulations are based on a 3D model of the reactor, with a detailed representation of structures inside and outside the vessel and different temperatures of the primary coolant, and require:

- STEP 1: 3D neutron sources models;
- STEP 2: 3D multigroup neutron flux maps of the structures of interest, considering as much as possible different neutron source distributions (i.e. different power distributions) and different loading patterns, average control rods position, average absorber concentration etc, or at least significant power distribution variations;
- STEP 3: Calculation of the residual activities for each structure or component of interest, taking into account the exact chemical composition of the materials and paying attention to impurities concentrations;
- STEP 4: Validation and continuous improvement of the calculation scheme comparing result with measurement of detectors/samples such as, for example, those provided by vessel fluence monitoring program.

Sogin (Società Italiana Gestione Impianti Nucleari) (Sogin, 2021b), the Italian company in charge of the decommissioning of the four Italian NPPs, established since 2019 a formal agreement with the Italian university consortium CIRTEN (Consorzio Interuniversitario per la Ricerca TEcnologica Nucleare) (CIRTEN, 2021) to carry out joint research activities in the field of NPP decommissioning. In the frame of that agreement, an activity regarding the development of innovative strategies for the dismantling of primary circuit components has been launched at Politecnico di Torino, which is member of CIRTEN.

The present paper summarizes a part of the work performed, specifically the development of a four-step calculation scheme whose aim is to evaluate the residual activation in the structures surrounding the core of the PWR belonging to the Enrico Fermi NPP, such as the RPV and RVIs.

More in detail, in this paper the developed scheme is used to assess the residual activation of a set of selected points of the thermal shield, an internal component of the reactor that was removed at the end of the first operating cycle. The investigated points are chosen in order to match those selected for two separate sampling campaigns that were carried out by ENEL in 1969 and in 1992 on the

thermal shield. This approach allows for a direct comparison between the measurements and the results of the calculation.

In the following section the development of calculation scheme is discussed, with a specific focus on each of the four steps. In the last section, the key results are presented and the main issues are discussed, together with the work which is planned for the future

## **2. Development of the calculation scheme**

In this section, the development of the calculation scheme is described. Similar schemes have been successfully used in the past to analyse activation phenomena (Culioli et al., 2016) (Janski, 2016) (Janski, 2019). The scheme consists in the following four steps, which are shown in Figure 1:

- A first Monte Carlo simulation, performed with the code Serpent 2 (Leppänen, 2015) in criticality mode, whose aim is to generate the neutron source term required for the second step;
- A second set of Monte Carlo simulations, again performed with Serpent 2, in external source mode and using variance reduction techniques, which take as input the previously calculated source and perform the accelerated transport of neutrons towards the selected regions of the thermal shield, where the integral neutron fluxes, i.e. the neutron fluxes integrated over the entire energy range, or the neutron spectra are calculated;
- A final set of activation calculations, performed with a deterministic approach with the code FISPACT-II (Sublet et al., 2017), whose aim is to evaluate the residual activation in the selected points. This step requires as input the previously calculated integral neutron fluxes and neutron spectra, plus some other essential information regarding the material composition and the irradiation history;
- Validation of the calculated results by comparison to the available measurements. The comparisons are performed using the ratio between the calculated specific activities and the measured ones (C/M ratio) for each point and each isotope considered.

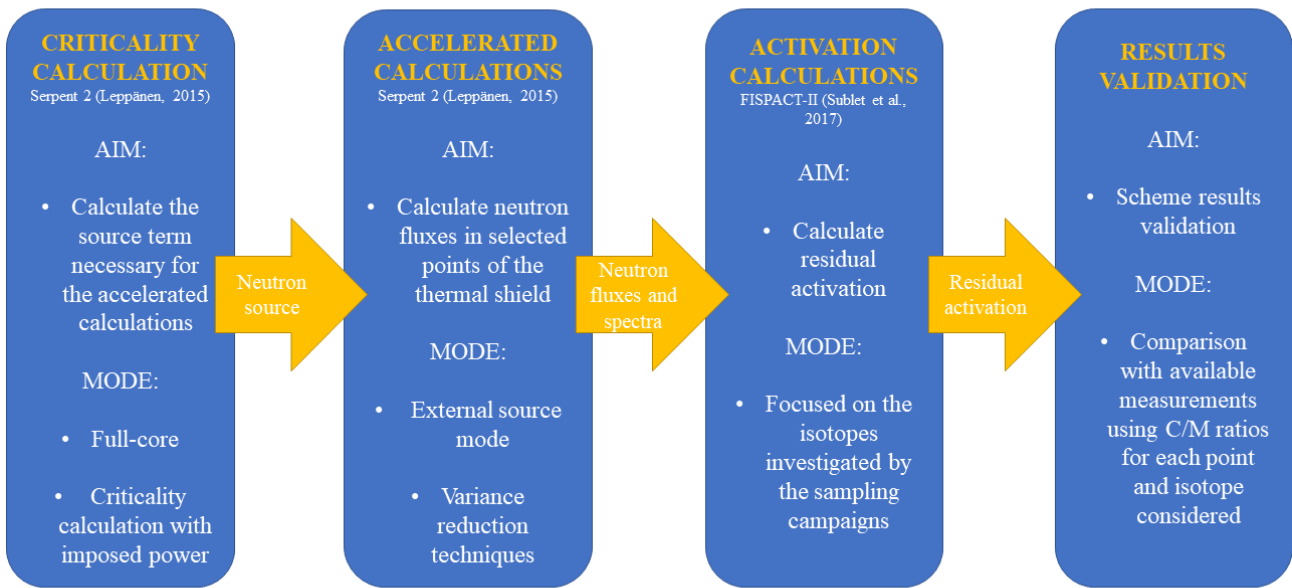


Figure 1: Calculation scheme adopted in this work.

This approach allows to reconstruct the behaviour of the reactor and to evaluate the residual activation of the structures affected by neutron irradiation. In this paper the scheme is applied to the analysis of the thermal shield after the first operating cycle of the Trino reactor: this choice is due to the availability of two separate sets of measurements on the residual activation of the component, which had been inserted between the core barrel and the RPV. It was later removed before the beginning of the second operating cycle, as the core itself underwent some major modifications involving both geometry and fuel enrichment.

The previously mentioned codes selected for the implementation of the scheme are Serpent 2 for the MC steps and FISPACT-II for the activation step. Serpent 2 (Leppänen et al., 2015) is a multi-purpose, three-dimensional continuous energy MC particle transport code developed by the VTT Technical Research Centre of Finland; FISPACT-II (Sublet et al., 2017) is a multi-physics, inventory and source-term code developed at the UK Atomic Energy Authority. It provides a large variety of advanced, predictive, temporal and spectral simulation methods using up-to-date nuclear data for both neutrons and other charged particles, such as electrons or protons. Similarly to ORIGEN, FISPACT-II is mainly used to solve sets of Bateman equations for inventory calculations, addressing phenomena such as material activation, transmutation, fuel depletion and radioactive decay.

### Setup of the Monte Carlo simulations

The numerical modelling of the neutron flux in the reactor core, useful to determine the activation source, can be approached through deterministic or stochastic methods. Deterministic methods are usually applied to solve some approximation of the transport equation, and rely on the discretization

of the variables involved in the transport process, such as space, energy, direction of flight and time (Ahn et al., 2019). Each cell of the generated mesh is characterised by constant properties (e.g. cross sections). Deterministic methods have often been used in the past for their reasonably small computational cost, especially when the neutron diffusion approximation and the computer technology available in the 90's are considered, i.e. when the Italian decommissioning process started. The Monte Carlo (MC) method, on the other hand, relies on aggregated information provided by the statistical sampling of a large number of particle histories. The neutron propagation and interaction phenomena are simulated accessing continuous energy cross section libraries and the complexity of the geometry can be retained to a high level of detail, thus eliminating the approximation introduced by the discretization process adopted in deterministic methods. For these reasons, MC codes allow for a representation of the transport mechanism closer to reality (Lux & Koblinger, 1991), and they have been effectively used in the past to investigate activation phenomena in structural components, (Love et al., 1995), (Johansson, 2012), (Schlömer et al., 2017), (Phlippen et al., 2018), (Ahn et al., 2019), (Šnirer et al., 2021). A large number of neutron histories can be required in order to yield statistically significant results, which can impact significantly on the processing power and the memory used.

## **2.1 Critical simulation: source generation (STEP 1)**

The first Monte Carlo simulation, performed in criticality mode, is designed to evaluate the neutron source term. The source file generated by this first step contains all the information related to the neutron source points, such as spatial coordinates, energy, direction of flight and statistical weights. This file is used in the second step to compute the accelerated transport of neutrons generated in the source points towards the regions of interest applying variance reduction techniques, which in Serpent 2 are implemented to be used in external source mode only (Leppänen, 2019).

A 3D geometrical and neutronic model of the reactor was created using the plant data provided by Sogin. The model includes the RPV, the internal stainless steel-liner of the RPV and all the RVIs, as can be seen in Figure 2. All components are modelled in detail, thanks to the information provided by technical drawings, including the more unusual features of this early 60s design such as the cruciform fuel followers of the control rods. The control rods are modelled as extracted from the core (and therefore the followers are modelled as inserted), to simulate nominal full power operation (870 MWth). The thermal shield, formed by a stainless-steel hollow cylinder of about 7.5 cm thickness, is positioned in the region between the core barrel and the RPV. Fuel enrichments and structural material compositions were provided by Sogin, the latter originally obtained through a combination of neutron activation analyses of unirradiated samples, data coming from literature and from the certifications provided by the materials producer. In order to provide a reasonably conservative estimate of the residual activation, no boron is dissolved in the coolant.

The modelled fuel pattern shown in Figure 2 is characterised by three concentric regions, with increasing enrichments moving from the centre towards the periphery of the core. This high leakage fuel pattern was responsible for a significant irradiation of the thermal shield, even if its presence in the reactor lasted only one operating cycle. The control rods cruciform followers, which are made by fuel rods themselves, share the same enrichment of the innermost region.

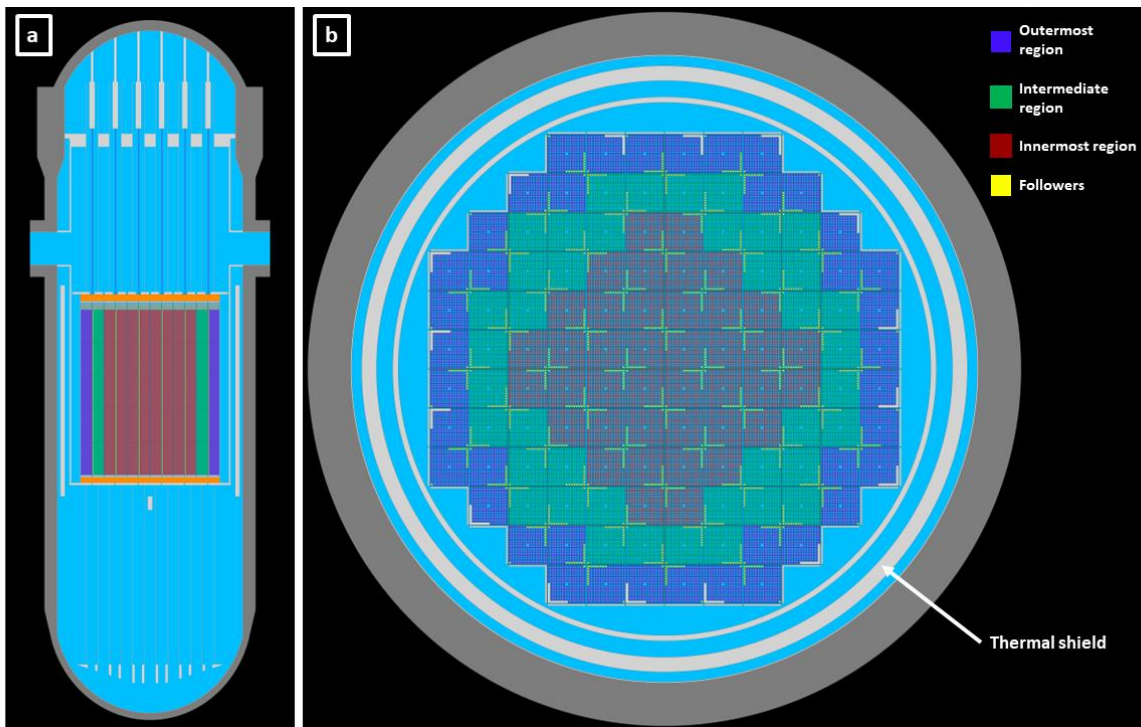


Figure 2: Vertical cross section (a) and horizontal (core midplane) cross section (b) of the reactor. The fuel of different composition is represented with different colors. Fuel followers are represented with a fourth different color, although sharing the same composition of the innermost fuel, for clarity.

## 2.2 External source simulations: accelerated transport and variance reduction techniques (STEP 2)

The second step of the calculation process with Serpent 2 is the neutron propagation from the reactor core to the surrounding thermal shield for the evaluation of the integral neutron flux in the selected points of the component and the neutron spectra, which are necessary for the subsequent activation analysis. As this step involves the propagation of neutrons through several centimetres of water and in some cases of stainless-steel, the problem of obtaining a sufficient statistic in the tallies in the shielded regions is relevant. The Serpent 2 code can perform neutron transport simulation with the aid of variance reduction (VR) techniques, which are adopted in this work to accelerate neutrons generated in the core towards the surrounding structures.

A set of 17 small spherical void detectors ( $r = 1$  cm) was defined to estimate the integral neutron flux using the track length estimator. The investigated points correspond to the ones selected for the sampling campaigns and are therefore located either on the inner or on the outer surface of the shield. Their coordinates are listed in Table 1, where  $z = 0$  cm corresponds to the middle of the active zone of the core and  $\theta = 0^\circ$  corresponds to the middle point of one of the sides of the core, as shown in Figure 3.

Table 1: Coordinates of the investigated points of the thermal shield.

| $\theta$ [°] | z [cm]  | Inner surface/outer surface |
|--------------|---------|-----------------------------|
| 0            | 172.35  | Inner surface               |
| 0            | 134.35  | Inner surface               |
| 0            | 102.35  | Inner surface               |
| 0            | 72.35   | Inner surface               |
| 0            | 39.35   | Inner surface               |
| 0            | 13.35   | Inner surface               |
| 0            | 12.35   | Inner surface               |
| 0            | 12.35   | Outer surface               |
| 0            | -21.65  | Inner surface               |
| 0            | -53.65  | Inner surface               |
| 0            | -93.65  | Inner surface               |
| 0            | -134.65 | Inner surface               |
| 0            | -170.65 | Inner surface               |
| 20           | 12.35   | Inner surface               |
| 20           | 12.35   | Outer surface               |
| 317.2        | 12.35   | Inner surface               |
| 317.2        | 12.35   | Outer surface               |

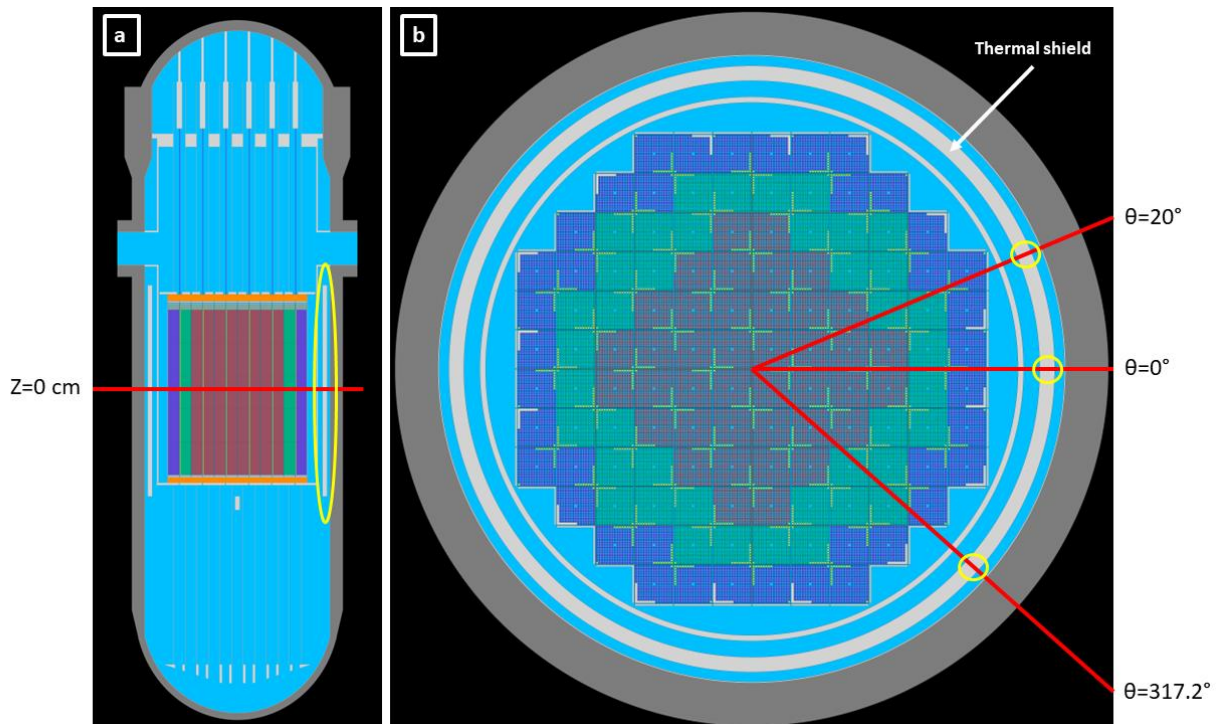


Figure 3: Vertical cross section (a) and horizontal (core midplane) section (b) of the reactor. The detector locations are highlighted with yellow circles.

Preliminary calculations performed at various points on the inner surface of the shield suggest that there is no significant change in the normalised neutron spectrum along the axial (z) and angular ( $\theta$ ) coordinates for most of the analysed points, probably due to the proximity of the component to the

core, as can be seen in Figure 4, where the spectra for different heights and for different angular positions are compared to the integral spectra. The graphs are basically superimposing, and the effect of the better statistics of the integral flux on the thermal and fast tails can be seen.

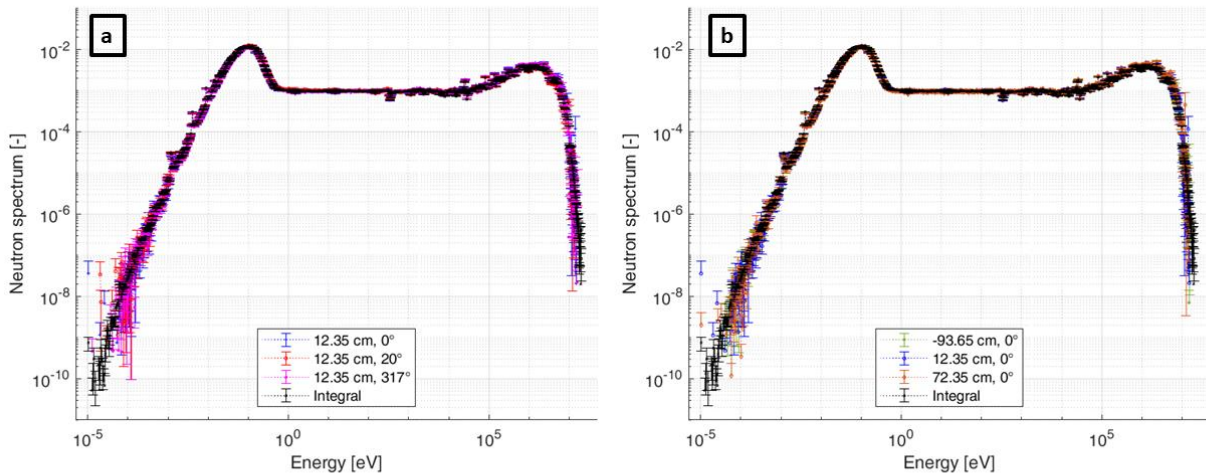


Figure 4: Neutron spectra on the internal surface of the shield at different angular (a) and axial (b) locations. All the spectra overlap for most energies, but in the high and low energy regions the integral spectrum is better defined.

For this reason, two spectra belonging to the inner and outer surface of the shield are calculated to investigate the residual activation of most of the analysed points, and both spectra are integrated along the shield height and the whole circumference. This approach allows for better statistics in the treatment of very high and low energy neutrons. The only two exceptions are the points at the very top and bottom of the shield, which are characterised by slightly different spectra due to local conditions that will be further discussed in section 2.3.4.

In this case the dependence of the neutron spectrum on the radial coordinate ( $r$ ) cannot be neglected: in fact, the thickness of the shield has a significant effect on the neutron energy distribution, as can be seen from Figure 5, where the neutron spectra on the inner and outer surface of the thermal shield are compared. The inner surface spectrum has a notably higher thermal peak than the outer surface one.

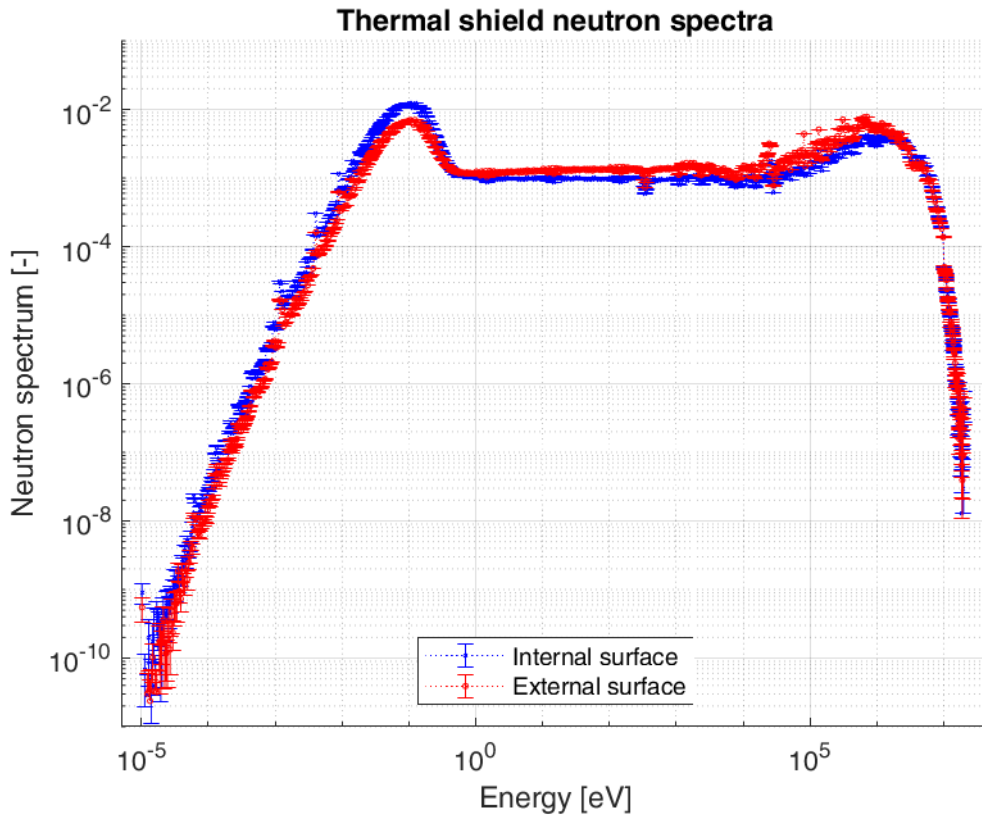


Figure 5: Neutron spectra on the internal and external surface of the thermal shield.

The acceleration model for the integral flux is tailored to the objective, in order to separately accelerate the particles towards the regions at different angular coordinates and at different heights. This approach allows to avoid accelerating particles towards too many different directions simultaneously, which could be counterproductive.

The variance reduction techniques implemented in Serpent 2 are based on standard Weight Window (WW) calculation schemes: a deterministic response matrix-based solver was developed at VTT and implemented to provide information on neutron importance considering the detector positions (Leppänen et al., 2017). This information is used to enhance the propagation of neutrons in some directions and hinder it in others, by means of two population control mechanisms known as “*russian roulette*” and “*splitting*”. Both mechanisms manipulate the statistical weight assigned to particles when they enter a new region of the mesh characterised by a different importance, without modifying the overall statistics of the phenomenon (Lux & Koblinger, 1991) (Pantelias Garcés, 2013).

The importance of the different cells is calculated by internal routines according to the user’s input. There are three importance generation methods that can be combined for an optimal result:

- Single detector;
- Multi detector;
- Global Variance Reduction (GVR).

The first two methods are quite similar and allow the generation of regions of greater importance where the user defines the detectors. Particles are then accelerated in the direction of one or more detectors and progressively removed from the opposing directions according to the above-mentioned russian roulette and splitting mechanisms. The drawback of the single and multi-detector techniques

is that they require a minimum amount of particles to reach the detectors before the acceleration starts (Leppänen, 2019). If the regions delimited by the detectors are shielded and/or distant from the source, it is possible that this minimum number is not reached, or that no particle arrives at all, causing a fatal error and the simulation failure. For this reason, a preliminary step is introduced in this scheme based on the Global Variance Reduction technique, which allows to generate importance maps that progressively populate with particles the whole geometry. A detector-specific acceleration is implemented afterwards for the final transport calculation. An example of a qualitative importance map is shown in Figure 6. This map was produced for the detector at the bottom of the shield with coordinates  $\theta = 0^\circ$  and  $z = -170.65$  cm

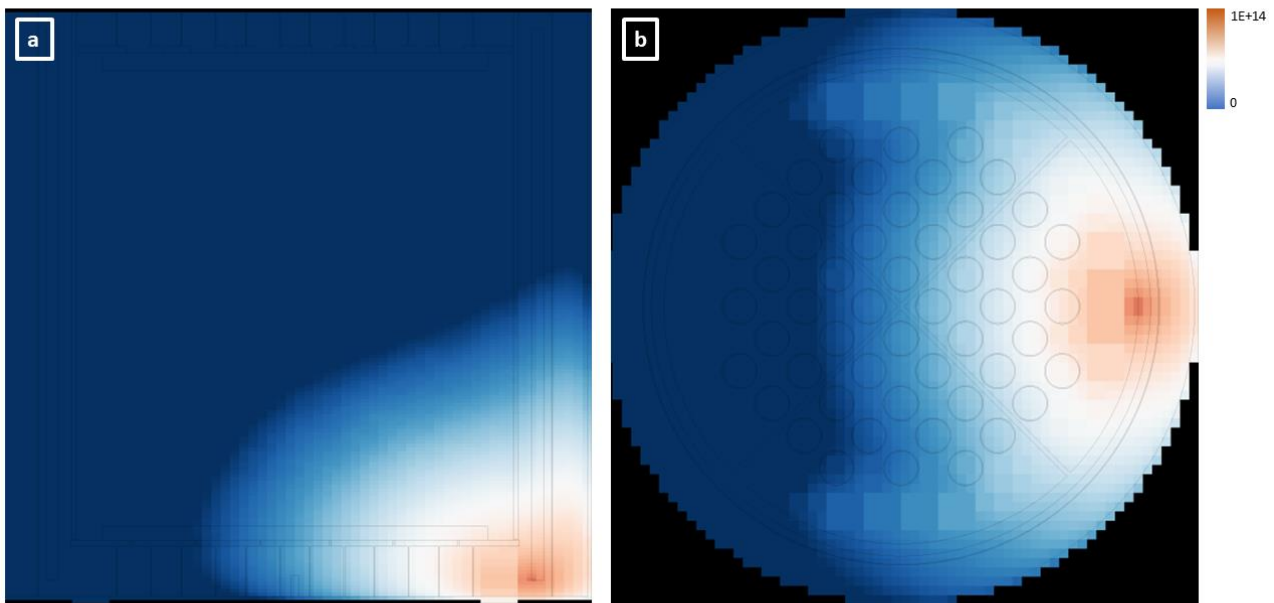


Figure 6: Neutron importance, evaluated by Serpent 2 for the acceleration scheme, for a XZ section (a) and XY (shield bottom) section (b) of the central part of the reactor. The warmer the color, the higher the cell importance. As can be seen from both pictures, the importance map is tailored to the specific detector selected, in order to enhance the neutron transport in the desired direction.

### 2.3 Activation calculation (STEP 3)

The third part of the calculation scheme involves a set of simulations to evaluate the residual activation of the selected set of points of the thermal shield. This type of calculation typically requires a lot of input data, which are briefly discussed in the following sections.

#### 2.3.1 Detailed material compositions, including impurities

Some impurities in the structural materials are typically a cause of concern, such as  $^{59}\text{Co}$  in carbon and stainless steels, which is easily transmuted into  $^{60}\text{Co}$  if exposed to a thermal neutron flux.  $^{60}\text{Co}$  is a strong gamma emitter (energy peaks at 1.173 and 1.332 MeV) with a half-life of 5.27 years, therefore it is one of the most important nuclides to be considered for radiation protection purposes during the development of the decommissioning plans. Since trace amount of cobalt do not significantly impact the mechanical and thermal properties of steel, the control of this impurity was often not considered a priority during the manufacturing stage of reactor components in the past. This

is also the main reason why the trace amounts of cobalt in steels used for different plants may vary by more than one order of magnitude (Evans et al., 1984). Other examples of trace nuclide in structural materials that may be cause of concern for decommissioning purposes are  $^{151}\text{Eu}$  and  $^{153}\text{Eu}$  in concrete (Ahn et al., 2019).

### 2.3.2 Reconstructed irradiation history and decay time

Knowing the operational history of the investigated reactor cycle is essential to evaluate the irradiation time. In order to correctly represent power variation and shutdowns, a simplified operational history formed by intervals at constant power is usually created starting from plant data. This process might be difficult if the reactor operated rather discontinuously and/or at many different power levels, which is indeed the case for the first operating cycle of the Trino reactor, see Figure 7 (Sogin, 1977b).

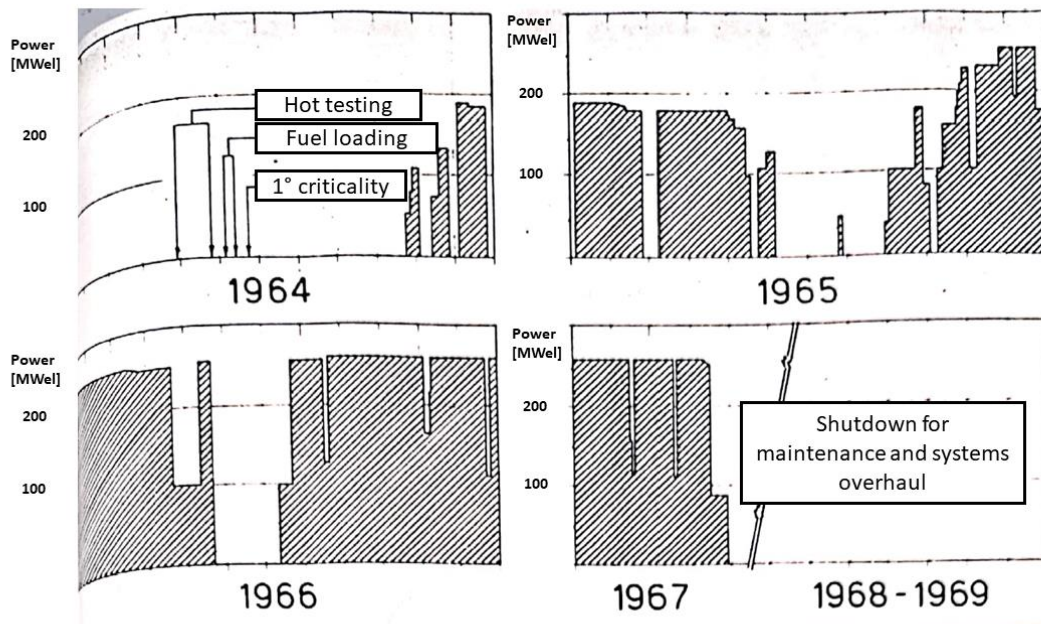


Figure 7: First operating cycle of the Trino reactor (Sogin, 1977b).

In the framework of this study, the simplified irradiation history used was suggested by Sogin documentation (Sogin, 1977a) and is presented in Table 2. It is formed by three irradiation periods at different power levels separated by two shutdowns.

Table 2: Simplified irradiation history used to reconstruct the first operating cycle of the Trino reactor.

| Interval | From       | To         | Irradiation time [d] | P/P <sub>max</sub> |
|----------|------------|------------|----------------------|--------------------|
| 1        | 21/10/1964 | 06/06/1965 | 225                  | 0.56               |
| 2        | 07/06/1965 | 31/08/1965 | 87                   | 0                  |
| 3        | 01/09/1965 | 20/05/1966 | 260                  | 0.75               |
| 4        | 21/05/1966 | 11/07/1966 | 53                   | 0                  |
| 5        | 12/07/1966 | 28/04/1967 | 295                  | 0.89               |

The decay time is the period between the end of the cycle and the measurement of the residual activation, and it is needed to consider the decrease in activity caused by radioactive decay. Two separate decay times were considered, as the sampling campaigns were performed in August 1969 and in February 1992:

- 28/04/1967 – 1/08/1969 for the first dataset;
- 28/04/1967 – 06/02/1992 for the second dataset.

### 2.3.3 Nuclear data

A large amount of nuclear data is required to perform activation calculations. Depending on the target of the study, cross sections for several different reactions and decay constants for many nuclides may be needed. In the framework of this work, the nuclear data library TENDL-2017 (PSI, 2022) has been adopted, and the main reactions of interest, based on the available measurements, are the ones that concur to the generation of the following isotopes:  $^{55}\text{Fe}$ ,  $^{60}\text{Co}$ ,  $^{59}\text{Ni}$ ,  $^{63}\text{Ni}$  and  $^{54}\text{Mn}$ . The first four isotopes are mainly generated by radiative capture of thermal neutrons by (n, $\gamma$ ) reactions, while the last one originates mainly from a neutron-proton (n,p) reaction that requires fast neutrons ( $E \geq 0.7$  MeV).  $^{55}\text{Fe}$  and  $^{54}\text{Mn}$ , while valuable for assessing the scheme performance, are not expected to be particularly relevant for the decommissioning of the Trino reactor, considering the amount of time passed since the shutdown, which occurred in 1987 and their short half-life of 2.74 years and 312 days, respectively (IAEA, 2021).

### 2.3.4 Neutron spectra and integral neutron flux

The intensity of the neutron flux and its energy distribution are the last two parameters required to perform activation calculations. Before the calculation itself, the cross sections have to be weighted on the incoming neutron flux spectrum: this weighting procedure is known as “collapse” and allows for the calculation of a single-energy group effective microscopic cross section:

$$\sigma_i^j = \sum_k \tilde{\sigma}_i^j(E_k) \Phi_n / \sum_k \Phi_n(E_k)$$

where the cross section for the nuclide  $j$  producing  $i$  depends on  $\tilde{\sigma}_i^j(E_k)$ , which is the cross section at projectile energy group  $k$ , and on  $\Phi_n(E_k)$ , which is the integrated projectile flux in energy group  $k$ . The sums are over all energy groups  $k$ .

The one-group effective cross sections are then used to evaluate the reaction rates once multiplied by the integral flux in the Bateman model:

$$\frac{dN_i}{dt} = \sum_j (\lambda_i^j + \sigma_i^j \Phi^{int}(t)) N_j$$

where the variation in nuclide population  $N_i$  is dependent on both reaction rates and decay phenomena, as  $\lambda_i^j$  is the decay constant of nuclide  $j$  transmuting into  $i$ .

As previously mentioned, a shorter or longer distance from the source, as well as the presence of different materials on the neutron trajectory, may cause a different energy distribution of the neutron flux. In the case of the thermal shield, the neutron spectrum appears to be the same along the angular

and axial coordinates for all the points analysed except two, probably due to the proximity of the component to the source. Integrating along those coordinates allows for a more detailed description of the neutron energy distribution, especially in the low ( $E \leq 0.001$  eV) and high ( $E \geq 1$  MeV) energy range. The latter in particular is important to assess the production of  $^{54}\text{Mn}$ , which is only produced from  $^{54}\text{Fe}$  by (n,p) reactions with fast neutrons. A poorly defined spectrum in the fast region, e.g. due to insufficient statistics, could lead to a poor prediction of the residual activation due to this isotope.

The two points previously introduced that are characterised by a slightly different spectrum are located at the very top ( $z = 172.35$  cm) and bottom ( $z = -170.65$  cm) of the shield. The spectra in those regions are slightly different compared to the rest of the component, as more water than steel is present in the surrounding volumes due to the shield geometry and sampling point selection.

A comparison between the integral and local spectra suggest that the use of the latter would imply a higher  $^{60}\text{Co}$  production compared to the integral spectrum, due to the higher thermal peak. Both the integral and local spectra are well defined in the thermal region, but statistical uncertainty affects the local spectra in the fast region, as can be seen in Figure 8.

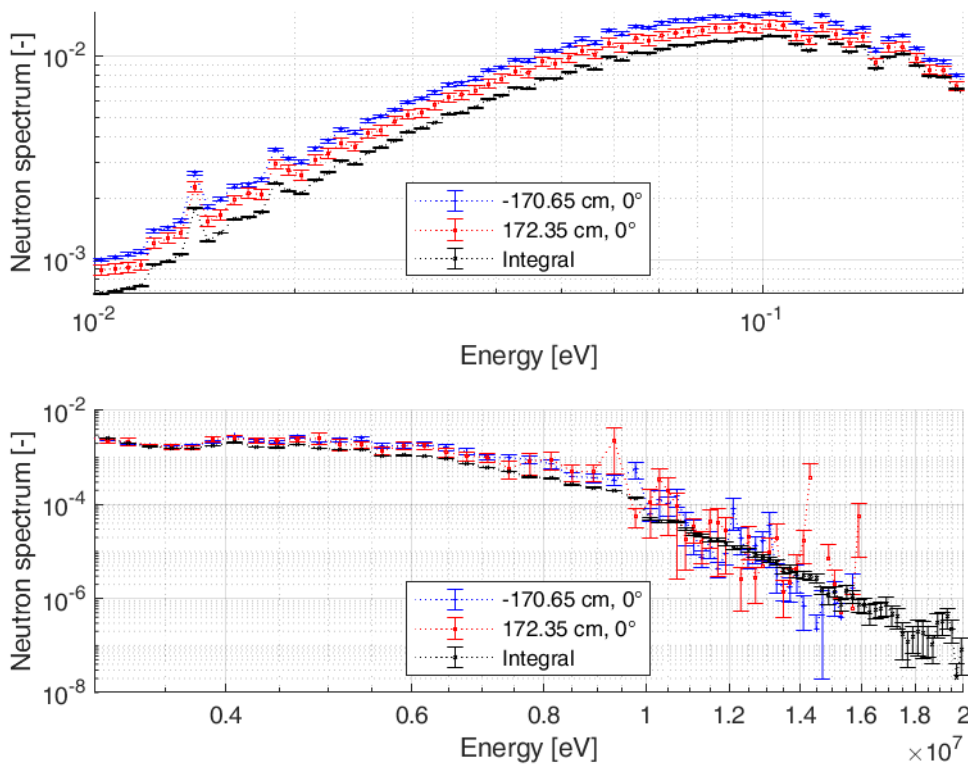


Figure 8: Thermal (top) and fast (bottom) neutron spectra of the points at the top and bottom of the shield

For this reason, the residual activation due to  $^{60}\text{Co}$  is reliable if calculated with the local spectra, but the same does not occur when  $^{54}\text{Mn}$  is considered, as the calculation is sensitive to the input spectrum and therefore to its statistical uncertainty. Considering the higher importance of  $^{60}\text{Co}$  with respect to  $^{54}\text{Mn}$  in the decommissioning efforts, for these two points the local spectrum was used in the activation calculation, in order to provide a more accurate  $^{60}\text{Co}$  estimate that considers the local effects, even if this means a less reliable  $^{54}\text{Mn}$  assessment. For all the other points, the use of the

integral spectrum does not significantly affect the  $^{60}\text{Co}$  estimate, since its thermal peak overlaps the one of the local spectra but, at the same time, a more precise  $^{54}\text{Mn}$  evaluation is possible as a result of the lower uncertainties in the fast region, as can be seen in Figure 9.

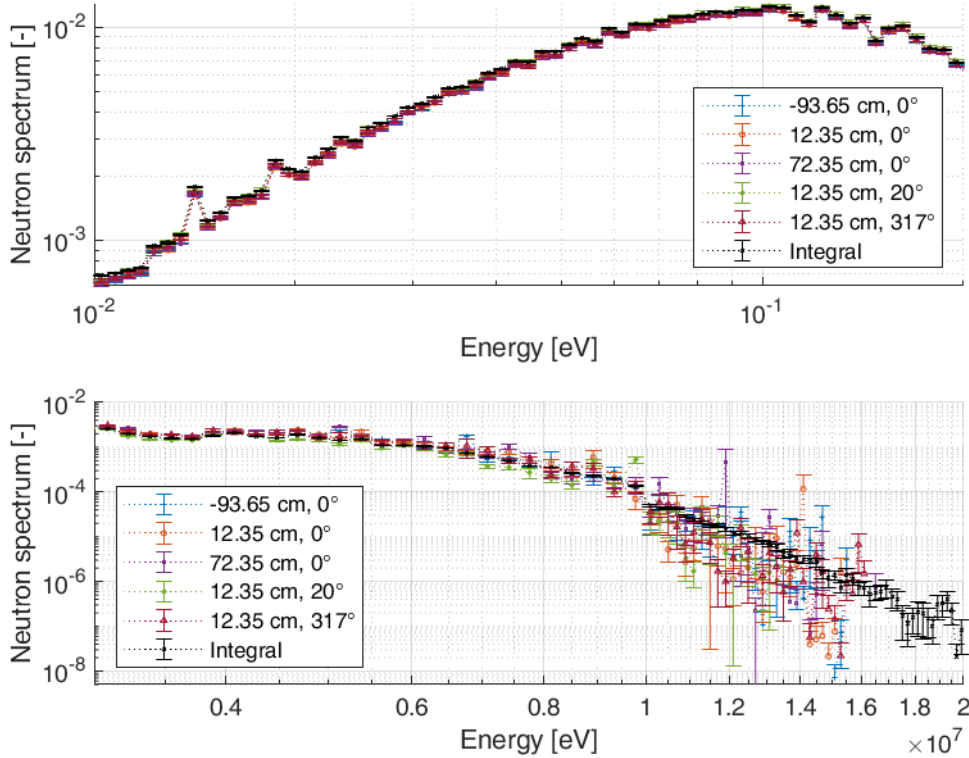


Figure 9: Thermal (top) and fast (bottom) neutron spectra of some of the other points located on the internal surface of the shield at different heights and angular coordinates

## 2.4 Results comparison and validation (STEP 4)

The results are presented in this section by means of the C/M ratio:

$$\frac{C}{M} = \frac{\text{Specific activity}_{\text{calculated}}}{\text{Specific activity}_{\text{measured}}} \quad (1)$$

a performance indicator that allows to compare the specific activities calculated by the scheme to those available from the database, for each point and for each isotope considered. C/M values in the range 1 – 10 are here considered acceptable, as they imply a conservative prediction of the specific activities, but not an excessive overestimation for decommissioning purposes (Tanaka et al., 2016) (Tanaka & Ueno, 2017). The range appears reasonable also considering what has been done in other works: (Schlömer et al., 2017) reported values in the 0.9 – 6.8 range for most of the isotopes considered, in many cases in agreement with the activation foil campaign discussed in (Pantelias &

Volmert, 2015); (Phlippen et al., 2018) and (Ahn et al., 2019) in Annex IV analysed several isotopes and reported values up to 7.7 and 7.9 respectively, in some locations. In a previous activation study performed for Sogin (Genova et al., 1995), values considered acceptable belonged to the interval 0.7 – 8.77. Discrepancies between the calculated and measured values are often due to a combination of different factors, such as uncertainties in the nuclear data, in the activation measurements, in the materials composition or in the operational history. If MC techniques are used, statistical uncertainty is involved as well.

### **2.4.1 1969 sampling campaign**

The first sampling campaign on the thermal shield occurred in August 1969. The component had been removed from the reactor at the end of the first operating cycle and subsequently stored in the adjacent pool. The campaign aimed mainly, but not exclusively, at evaluating the axial profile of the residual activation due to  $^{60}\text{Co}$  and  $^{54}\text{Mn}$  on the inner side of the shield, at  $\theta = 0^\circ$ . Moreover, two points belonging to the inner and outer surface of the shield at  $\theta = 317.2^\circ$ , and a single point belonging to the outer surface at  $\theta = 0^\circ$ , were considered (ENEL S.p.a., 1993). It is important to highlight the fact that these data were collected for industrial purposes and a thorough description of how the measurements were performed, as well as an error bar, is missing. For this reason, the only error bars reported are the ones belonging to the results calculated by FISPACT-II.

#### **2.4.1.1 Axial distribution of the residual activation caused by $^{54}\text{Mn}$ and $^{60}\text{Co}$ at $\theta = 0^\circ$**

The axial distribution of the residual activation caused by  $^{54}\text{Mn}$  and  $^{60}\text{Co}$  on the internal surface of the shield is shown in Figure 10, and the axial distribution of the respective C/M values is shown in Figure 11.

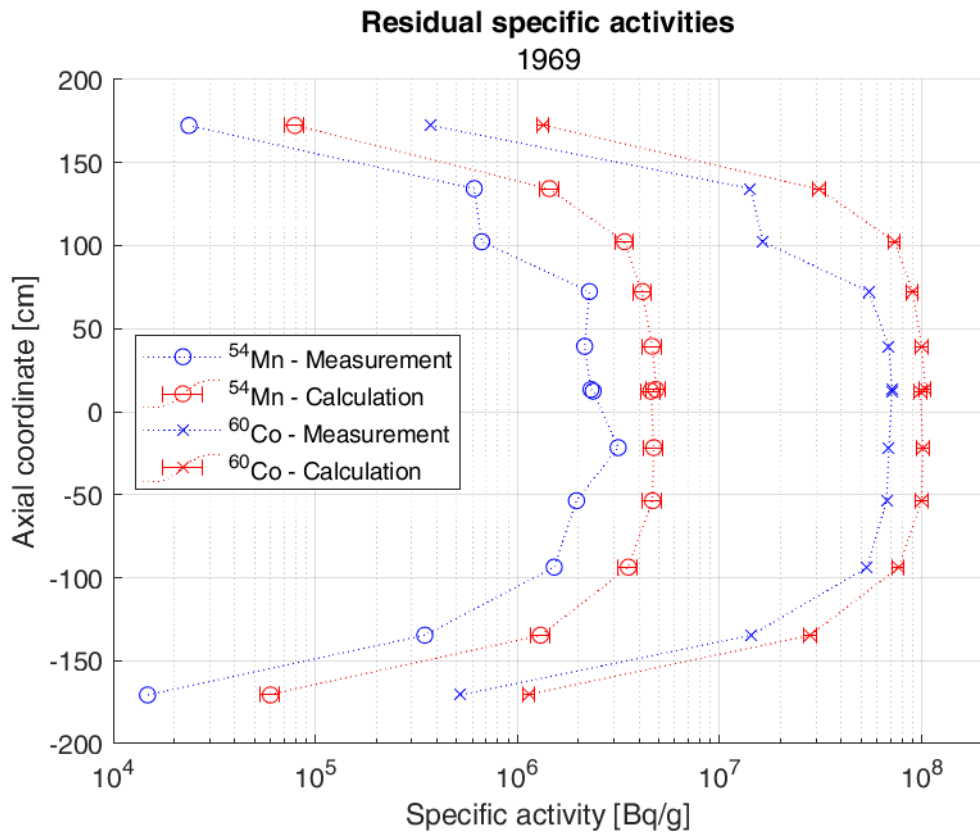


Figure 10: Axial distribution of the specific activity on the inner surface of the shield caused by  $^{54}\text{Mn}$  and  $^{60}\text{Co}$  at  $\theta = 0^\circ$ . Measurements from the 1969 sampling campaign.

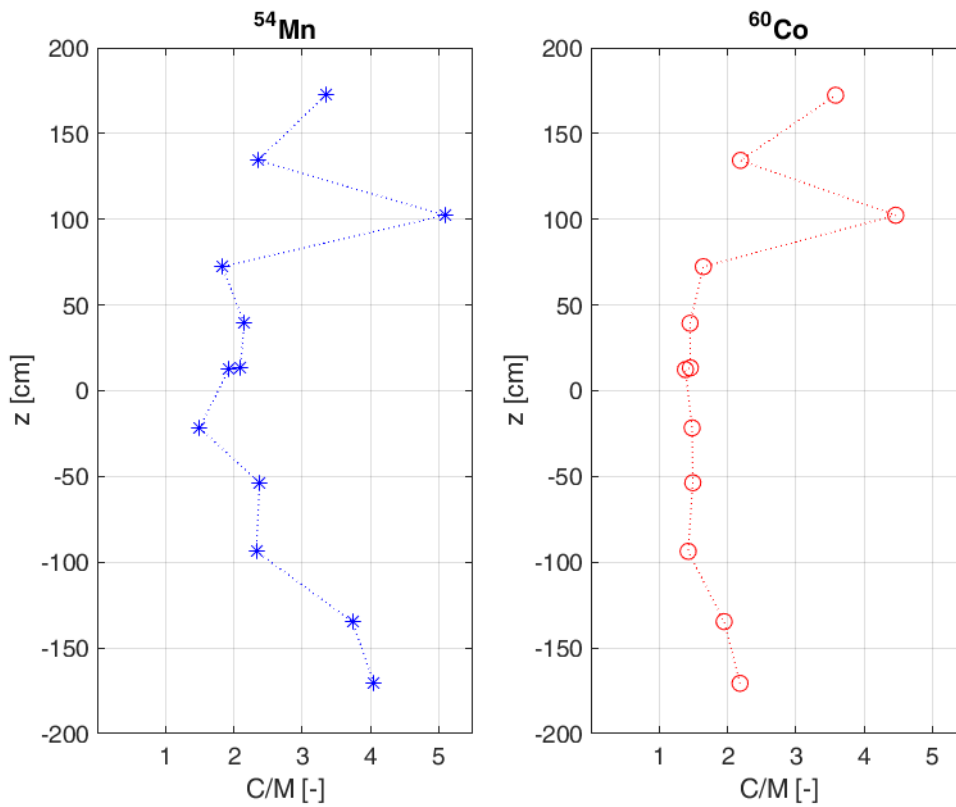


Figure 11: Axial distribution of the C/M values for the isotopes considered

As can be seen from Figure 11, all the values of the C/M ratio for both isotopes belong to the 1 – 10 range of acceptability. The anomaly at  $z = 102.35$  cm could be possibly related to some issues with the sample and/or the measurement, since it occurs similarly for both isotopes. Overall, however, the results can be considered satisfying and conservative, since the calculated residual activations are slightly higher than the measured ones, and even considering the error bars the C/M ratio is never lower than 1. As previously mentioned,  $^{54}\text{Mn}$  is not expected to be a nuclide of concern for the dismantling of the Trino reactor: since the isotope half-life is 312 days, its current presence 35 years after shutdown is negligible, and in fact it was already not measurable in 1992, when the second sampling campaign occurred (ENEL S.p.a., 1993).  $^{60}\text{Co}$  is a much more relevant nuclide, due to its gamma rays emission: its presence requires a careful and detailed radiation protection plan for all the phases of the dismantling activity (e.g. vessel and internals segmentation, transport), in order to ensure that the dose to the workers is as low as reasonably achievable in agreement with the ALARA principle.

#### 2.4.1.2 Other local values of the residual activation on the thermal shield surfaces

Only one sample was taken from the outer surface of the shield at  $\theta = 0^\circ$ , at the same height of one of the internal points ( $z = 12.35$  cm). The results of the comparison are reported in Table 3.

Table 3: Residual activation caused by  $^{54}\text{Mn}$  and  $^{60}\text{Co}$  on the external surface of the shield, at  $z = 12.35$  cm and  $\theta = 0^\circ$ . Measurements from (ENEL S.p.a., 1993).

| Isotope          | Measurement [Bq/g] | Calculation [Bq/g] | Calculation error [%] | C/M  |
|------------------|--------------------|--------------------|-----------------------|------|
| $^{54}\text{Mn}$ | 9.25E+05           | 1.20E+06           | 10.89                 | 1.30 |
| $^{60}\text{Co}$ | 1.41E+07           | 1.93E+07           | 8.02                  | 1.37 |

There is a good agreement between the scheme results and the measurements. The C/M values appear to be satisfactory on the outer surface of the shield as well. The specific activity caused by both isotopes is correctly simulated and similarly to the other points discussed, the results are proven to be conservative.

Two samples were taken at  $\theta = 317.2^\circ$ , one on the inner and one on the outer side of the shield. They were both taken at  $z = 12.35$ , as was the case for the internal and external points investigated at  $\theta = 0^\circ$ . Unfortunately, only measurements of  $^{60}\text{Co}$  are available for these two points. The results of the comparison are reported in Table 4.

Table 4: Residual activation caused by  $^{60}\text{Co}$  on the internal and external surface of the thermal shield, at  $z = 12.35$  cm and  $\theta = 317.2^\circ$ . Measurements from (ENEL S.p.a., 1993)

| Position | Measurement [Bq/g] | Calculation [Bq/g] | Calculation error [%] | C/M  |
|----------|--------------------|--------------------|-----------------------|------|
| Internal | 5.77E+07           | 1.14E+08           | 7.01                  | 1.98 |
| External | 1.48E+07           | 2.22E+07           | 8.02                  | 1.50 |

The overall performance in the evaluation of the residual activation measured in 1969 can be considered satisfactory for both  $^{54}\text{Mn}$  and  $^{60}\text{Co}$ , as all the C/M ratios calculated belong to the interval of acceptability proposed. In most cases, specially as can be seen for  $^{60}\text{Co}$  in different regions of the shield, discrepancies are generally within a factor of 2, which highlight a good scheme performance.

#### 2.4.2 1992 sampling campaign

The second sampling campaign on the thermal shield occurred in February 1992. This campaign aimed at evaluating the specific activities caused not only by  $^{60}\text{Co}$ , but also by  $^{55}\text{Fe}$ ,  $^{59}\text{Ni}$  and  $^{63}\text{Ni}$ .

As previously mentioned,  $^{55}\text{Fe}$  has a half-life of 2.74 years, which implies that its concentration halved more than 20 times since the thermal shield was removed from the reactor in 1967, and about 11 times since the second sampling campaign. The current specific activity due to  $^{55}\text{Fe}$  in the thermal shield is therefore expected to be less than  $1/2000$  ( $1/2^{11} = 1/2048$ ) of that measured in 1992.  $^{55}\text{Fe}$  might be of more interest in the future dismantling of carbon steel components, such as the RPV, given the larger share of iron in the composition and the longer irradiation period.

$^{59}\text{Ni}$  and  $^{63}\text{Ni}$  are two of the most relevant isotopes in decommissioning activities, mainly due to the high share of nickel in stainless steel components, and due to their long half-lives.  $^{59}\text{Ni}$  is also a significant gamma emitter, due to a rather complicated decay scheme that originates, about once every thousand decays, a cascade of gamma rays up to 1.08 MeV (Evans et al., 1984).  $^{59}\text{Ni}$  has a half-life of 76000 years, while  $^{63}\text{Ni}$  of around 100 years, which implies that their decay will be slower over time than the other isotopes (e.g.  $^{60}\text{Co}$ ), and that the overall activity of the material will be dominated by these two nuclides for quite some time.

The activity caused by  $^{59}\text{Ni}$  and  $^{63}\text{Ni}$  is relevant in waste classification procedures, as it is one of the parameters the Italian regulation considers to define low- and intermediate-level waste (Italian Ministry of Environment, 2015). More in detail, a waste package belongs to the low-level waste (LLW) category if, among other parameters such as total activity and presence of other long-lived isotopes, the residual activation due to  $^{59}\text{Ni}$  and  $^{63}\text{Ni}$  is lower than 40 kBq/g. A higher value would place the waste package in the intermediate-level waste (ILW) category, regardless of the other parameters. As previously mentioned,  $^{54}\text{Mn}$  was not considered in this case because its presence was already not measurable in 1992 due to the very short half-life.

Only two points were sampled during this campaign, at  $\theta = 20^\circ$  and  $z = 12.35$ , on the internal and on the external surface of the shield (Sogin, 2021a). The measurement of the specific activities of  $^{55}\text{Fe}$ ,  $^{59}\text{Ni}$  and  $^{63}\text{Ni}$  allowed to test the scheme performance for the evaluation of these isotopes as well. Moreover, the 1992 dataset reports the error bars of the values, which allow more precise comparisons.

The results of the comparisons are reported in Figures 12 and 13.

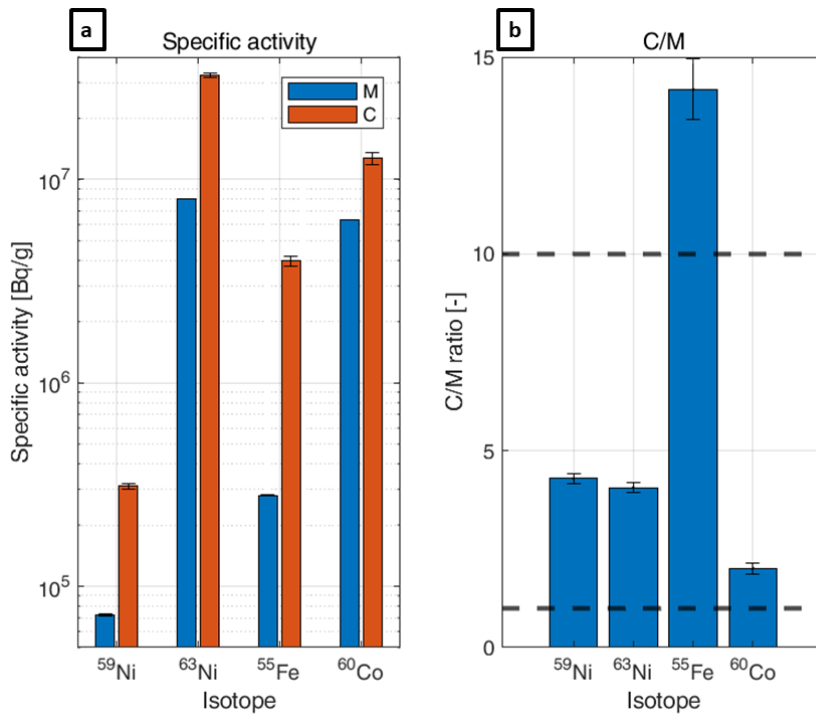


Figure 12: Computed (C) vs. measured (M) specific activities (a), and C/M ratios (b), caused by  $^{59}\text{Ni}$ ,  $^{63}\text{Ni}$ ,  $^{55}\text{Fe}$  and  $^{60}\text{Co}$  on the internal surface of the thermal shield, at  $z = 12.35$  cm and  $\theta = 20^\circ$ .

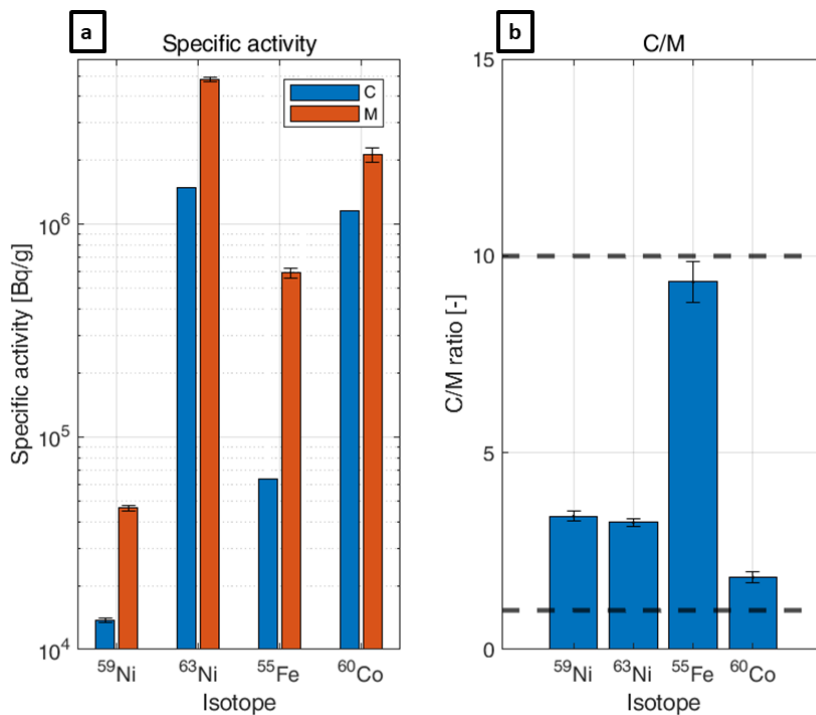


Figure 13: Computed (C) vs. measured (M) specific activities (a), and C/M ratios (b), caused by  $^{59}\text{Ni}$ ,  $^{63}\text{Ni}$ ,  $^{55}\text{Fe}$  and  $^{60}\text{Co}$  on the external surface of the thermal shield, at  $z = 12.35$  cm and  $\theta = 20^\circ$ .

As can be seen from both Figures 12 and 13, the results for the residual activities caused by  $^{59}\text{Ni}$ ,  $^{63}\text{Ni}$  and  $^{60}\text{Co}$  can be considered satisfactory, since they provide a reasonably conservative estimate. On

the other hand, the concentration of  $^{55}\text{Fe}$  is overestimated on the internal point, as the value of C/M for this isotope is above the upper boundary of the acceptability interval (1-10). Considering the overall good prediction of all the other isotopes, this might be due to a lower share of iron in the composition of the actual stainless steel compared with the one adopted in this analysis. As previously discussed,  $^{55}\text{Fe}$  is not expected to be the main source of residual activation in the future, and the other three isotopes play a more significant role in the development of the decommissioning plan and waste classification.

### 3. Conclusions and perspectives

In order to evaluate the residual activation of the structures of the Trino reactor, a four-step calculation scheme was developed. The scheme can be adapted to the analysis of the overall lifetime of a thermal reactor, provided the proper geometry, fuel compositions and operational history. The first step consists of a Monte Carlo simulation needed to generate the neutron source term, which is then used in the second step, a set of several Monte Carlo simulations in which neutrons are transported with the help of variance reduction techniques towards the surrounding structures. The third step evaluates the residual activation in the irradiated components, and in the fourth step a validation of the calculated results with available measurements is performed. The geometrical and neutronic model of the reactor is tailored on the first operating cycle of the reactor, in order to take advantage of the data provided by two separate sampling campaigns, in 1969 and in 1992, which were aimed at evaluating the residual activation of the thermal shield, an internal component that was removed afterwards. The focus in this paper is the evaluation of the residual activation caused by the five isotopes investigated in the sampling campaigns:  $^{55}\text{Fe}$ ,  $^{54}\text{Mn}$ ,  $^{60}\text{Co}$ ,  $^{59}\text{Ni}$  and  $^{63}\text{Ni}$ .

The dataset of 1969 only focused on  $^{54}\text{Mn}$  and  $^{60}\text{Co}$ , and does not provide error bars for the measurements. The dataset of 1992 reports the residual activation of only two points, but more isotopes were analysed:  $^{55}\text{Fe}$ ,  $^{60}\text{Co}$ ,  $^{59}\text{Ni}$  and  $^{63}\text{Ni}$ . Moreover, error bars are available. This allows to evaluate the performance of the scheme on a broader range of nuclides, although only  $^{60}\text{Co}$ ,  $^{59}\text{Ni}$  and  $^{63}\text{Ni}$  are expected to be relevant for decommissioning activities.

The scheme performs reasonably well and reproduces almost all the measurements of both datasets with a satisfying accuracy. All results are reasonably conservative and belong to the acceptability interval proposed ( $1 < C/M < 10$ ), with the only exception of the specific activity of  $^{55}\text{Fe}$  calculated for the point on the internal surface at  $z = 12.35$  cm and  $\theta = 20^\circ$ , which is slightly overestimated. The overestimation may be due to a lower precursor concentration in the stainless-steel alloy used compared to the one modelled, but it is not severe and it is not expected to be particularly relevant during the decommissioning phase, as the isotope has a short half-life and its concentration nowadays is already a small fraction of the original one. In most cases, specially for  $^{60}\text{Co}$ , the calculated specific activities are less than a factor 2 higher than the measured ones, which implies a good scheme performance. The comparisons with the 1969 data had to be performed without considering measurement errors, which highlights the difficulty of working with legacy data gathered mainly for industrial needs, lacking a thorough description of the methods used. Even considering this drawback, the scheme correctly estimates the specific activities caused by the most relevant isotopes in decommissioning here analysed:  $^{60}\text{Co}$  for what concerns the radiation protection plan development,  $^{59}\text{Ni}$  and  $^{63}\text{Ni}$  for the waste characterization. It also correctly predicts the specific activities caused by  $^{54}\text{Mn}$  and  $^{55}\text{Fe}$ , although the latter is on one occasion slightly overestimated.

The results of the simulation scheme are affected by the same series of uncertainties mentioned in section 2.4, which arise from different parameters that are involved in the evaluation of residual activation. Uncertainties in the material composition, in the measurements and in the irradiation time could play a role in the final overestimation of the results, as well as other sources of uncertainties such as statistics in the Monte Carlo simulations and, more in general, nuclear data.

A major overhaul of the core occurred after the first cycle, to improve the performance of the reactor. Those modifications included the removal of the shield, a different refuelling pattern, the substitution of the corner fuel assemblies with dummies, the substitution of the fuel followers with zircaloy ones and a general increase of the fuel enrichments. For all these reasons, the geometrical and neutronic model in its current form cannot be used to analyse the other operating cycles of the reactor, but we plan to include the implementation of those changes, in order to expand its applicability in the future. More in detail, the aim would be to evaluate the axial profile of the residual activation of the RPV and of the RPV stainless steel liner. This would provide helpful information for the development of the segmentation plan of the component, as some parts further away from the core are expected to be weakly activated or treatable as conventional waste due to negligible activation, which could lead to significant savings.

#### 4. Acknowledgements

This work was developed in the framework of the collaboration between CIRTEN (Consorzio Interuniversitario per la Ricerca TEcnologica Nucleare, which includes Politecnico di Torino) and Sogin (Società Italiana Gestione Impianti Nucleari), which sponsored a temporary position (assegnista di ricerca) at Politecnico di Torino in 2019-2021 to work on decommissioning related issues.

Computational resources were provided by HPC@POLITO, a project of Academic Computing within the Department of Control and Computer Engineering at the Politecnico di Torino (<http://www.hpc.polito.it>)

#### 5. References

Ahn, S., Asghar, M., Babcsany, B., Blideanu, V., Boursier, N., Czifrus, S., Dulama, C., Janski, S., Keyvani Ghamsari, M., Korotkov, A., Ljubenov, V., Maksimovic, I., Mostashiri, S., Narkunas, E., Nurarni, E., Otvos, N., Posivak, E., Reisenweaver, D., Runevall, O., ... Vasari, I. (2019). Methodologies for Assessing the Induced Activation Source Term for Use in Decommissioning Applications. *IAEA Safety Reports Series, 95*. [https://www-pub.iaea.org/MTCD/Publications/PDF/P1823\\_web.pdf](https://www-pub.iaea.org/MTCD/Publications/PDF/P1823_web.pdf)

CIRTEN. (2021). *CIRTEN*. <http://www.cirten.it/>

Culioli, M., Chapoutier, N., Barbier, S., & Janski, S. (2016). State of the art of Monte Carlo technics for reliable activated waste evaluations. *Predec 2016*, 2–10.

ENEL S.p.a. (1993). *Caratterizzazione radiologica dell'impianto: analisi radiochimiche e radiometriche di componenti attivati*.

- Evans, J. C., Lepel, E. L., Sanders, R. W., Wilkerson, C. L., Silker, W., Thomas, C. W., Abel, K. H., & Robertson, D. R. (1984). *Long-Lived Activation Products in Reactor Materials—NUREG/CR-3474*.
- IAEA. (2021). *Nuclear Data Services*. <https://www-nds.iaea.org/>
- IAEA. (2022). *Power Reactor Information System - PRIS*. <https://pris.iaea.org/pris/>
- Italian Ministry of Environment. (2015). *Decreto 7 agosto 2015 - Classificazione dei rifiuti radioattivi, ai sensi dell'articolo 5 del decreto legislativo 4 marzo 2014, n. 45*. [https://www.mite.gov.it/sites/default/files/dim\\_07\\_08\\_2015\\_classificazione\\_rifiuti\\_radioattivi.pdf](https://www.mite.gov.it/sites/default/files/dim_07_08_2015_classificazione_rifiuti_radioattivi.pdf)
- Janski, S. (2016). Using Green's Functions to Compute 3 Dimensional Neutron Flux Maps. *WM2016 Conference*, 1–14.
- Janski, S. (2019). First step in validating the radiological inventories of the current French nuclear fleet. *WM2019 Conference*, 1–8.
- Johansson, L. (2012). Possible means to manage and store the BKAB RPV. *OECD NEA*. [https://inis.iaea.org/collection/NCLCollectionStore/\\_Public/45/073/45073553.pdf](https://inis.iaea.org/collection/NCLCollectionStore/_Public/45/073/45073553.pdf)
- Leppänen, J. (2015). Serpent – a Continuous-energy Monte Carlo Reactor Physics Burnup Calculation Code: User's Manual. *VTT*. [http://montecarlo.vtt.fi/download/Serpent\\_manual.pdf](http://montecarlo.vtt.fi/download/Serpent_manual.pdf)
- Leppänen, J. (2019). Response Matrix Method–Based Importance Solver and Variance Reduction Scheme in the Serpent 2 Monte Carlo Code. *Nuclear Technology*, 205(11), 1416–1432. <https://doi.org/10.1080/00295450.2019.1603710>
- Leppänen, J., Pusa, M., Viitanen, T., Valtavirta, V., & Kaltiaisenaho, T. (2015). The Serpent Monte Carlo code : Status, development and applications in 2013. *Annals of Nuclear Energy*, 82, 142–150. <https://doi.org/10.1016/j.anucene.2014.08.024>
- Leppänen, J., Viitanen, T., & Hyvönen, O. (2017). Development of a Variance Reduction Scheme in the Serpent 2 Monte Carlo Code. *M&C 2017, September*.
- Love, E. F., Pauley, K. A., & Reid, B. D. (1995). Use of MCNP for characterization of reactor vessel internals waste from decommissioned nuclear reactors. *Idaho National Engineering Laboratory*.
- Lux, I., & Koblinger, L. (1991). *Particle Transport Methods : Neutron and Photon Calculations*. CRC Press.
- Pantelias Garcés, M. (2013). *Activation Neutronics for the Swiss Nuclear Power Plants*. 21623, 12–19.
- Phlippen, P. W., Schlömer, L., Nekipelov, M., Vallentin, R., Lukas, B., Palm, S., & Mispagel, T. (2018). Numeric determination and validation of neutron-induced radioactive nuclide inventories for decommissioning and dismantling of light water reactors. *Nuclear Technology*, 201(1), 66–79. <https://doi.org/10.1080/00295450.2017.1399039>
- PSI. (2022). *TENDL-2017*. [https://tendl.web.psi.ch/tendl\\_2017/tendl2017.html](https://tendl.web.psi.ch/tendl_2017/tendl2017.html)
- Schlömer, L., Phlippen, P. W., & Lukas, B. (2017). Activation calculation for the dismantling and decommissioning of a light water reactor using MCNP<sup>TM</sup> with ADVANTG and ORIGEN-S.

*EPJ Web of Conferences*, 153. <https://doi.org/10.1051/epjconf/201715305020>

Šnirer, M., Slugeň, V., Macáček, M., Křištofová, K., Hausner, P., Farkas, G., & Hinca, R. (2021). Validation of Monte Carlo activation calculation for V1 NPP reactor concrete shaft. *Annals of Nuclear Energy*, 163. <https://doi.org/10.1016/j.anucene.2021.108556>

Sogin. (1977a). *Misure di attività specifica su un campione del rivestimento interno del recipiente a pressione della centrale elettronucleare di Trino - Valutazione dei flussi neutronici.*

Sogin. (1977b). *Rapporto Decennale sullo Stato di Conservazione di Trino.*

Sogin. (2021a). *Private communications.*

Sogin. (2021b). *Sogin.* <https://www.sogin.it/it>

Sublet, J. C., Eastwood, J. W., Morgan, J. G., Gilbert, M. R., Fleming, M., & Arter, W. (2017). FISPACT-II: An Advanced Simulation System for Activation, Transmutation and Material Modelling. *Nuclear Data Sheets*, 139, 77–137. <https://doi.org/10.1016/j.nds.2017.01.002>

Tanaka, K. ichi, & Ueno, J. (2017). Development of a reliable estimation procedure of radioactivity inventory in a BWR plant due to neutron irradiation for decommissioning. *EPJ Web of Conferences*, 05019(153), 1–6.

Tanaka, K. ichi, Ueno, J., & Chiba, S. (2016). Estimation of a boundary to distinguish between radioactive materials and non-radioactive materials around a Main Steam line and a Feed Water line in a Biological Shielding Wall of a BWR for decommissioning. *Progress in Nuclear Energy*, 93, 371–385. <https://doi.org/10.1016/j.pnucene.2016.08.021>